Revista Mexicana de Astronomía y Astrofísica, **44**, 71–83 (2008)

A DYNAMICAL MODEL FOR THE SPIRAL GALAXY NGC 3359

M. Rozas

Instituto de Astronomía
Universidad Nacional Autónoma de México, Ensenada, B. C., Mexico

Received 2007 June 12; accepted 2007 November 8

RESUMEN

En este trabajo, con simulaciones numéricas del medio interestelar, determinamos el patrón de velocidad y construimos un modelo dinámico para NGC 3359. Ésta es una galaxia espiral fuertemente barrada y estructuralmente compleja, incluyendo una zona anular con fuerte formación estelar. Presentamos simulaciones numéricas auto-consistentes del gas molecular de NGC 3359, y usando el potencial derivado de una imagen en la banda I, encontramos los parámetros responsables de la cinemática y de la morfología del gas observado. Los mejores resultados se han obtenido con un modelo con dos patrones de velocidad diferentes: la región central (hasta 15″) que corresponde a la barra nuclear rota con una Ω_s = 100 km s^{-1} kpc^{-1}; y la barra principal, junto con la espiral externa, desacopladas de la región nuclear, que rota con una velocidad angular, Ω_p = 27 km s^{-1} kpc^{-1}. Este modelo reproduce bien la compleja estructura en Hα de la galaxia en la zona interna, la cual no puede ser explicada con un único patrón de velocidad.

ABSTRACT

In this work we have determined a dynamical model for NGC 3359. This is a strongly barred spiral galaxy with a complex structure, within which we can see an annular zone of intense star formation. In this work we present self consistent numerical simulations of molecular gas in NGC 3359; and using the potential derived from an I band image, we attempt to find the parameters responsible for the kinematics and morphology of the observed gas. The best results are obtained for a two pattern speed model: the central region (up to 15″) corresponding to the nuclear bar which rotates with a Ω_s=100 km s^{-1} kpc^{-1}; and the main bar + outer spiral, decoupled from the nuclear region, which rotates with a angular velocity, Ω_p = 27 km s^{-1} kpc^{-1}. The model successfully reproduces the complex structure in Hα of the galaxy in the internal 20″ zone, which cannot really be explained with a unique mode pattern.

Key Words: galaxies: individual (NGC 3359) — galaxies: kinematics and dynamics — galaxies: spiral

1. INTRODUCTION

Interest in barred galaxies has increased in the past few decades as infrared images have demonstrated, in the majority of disc systems, the existence of an oval component or a bar component. Bars have been shown to be one of the possible mechanisms responsible for density waves. In addition, through numerical simulations, it has been possible to prove that a weak bar can produce a spiral perturbation in the gaseous component of the system and provoke strong torques which transfer the angular moment outward (Sanders & Huntley 1976; Combes & Gerin 1985).

There is a substantial number of disk galaxies which show double bars (e.g., Shaw et al. 1995; Friedli et al. 1996; Erwin & Sparke 1999; Kenney 1998; Maciejewski & Sparke 2000; Maiolino et al. 2000). The primary bars, which define the galactic morphology, extend over several kpcs, and the secondary (nuclear) bars, typically extend over less than 1 kpc.

The patterns in grand design isolated galaxies can be explained in general through a well defined and predominant wave driven by a bar. A bar itself is a standing m=2 wave mode, that in the models shares the same pattern speed as the spiral structure. Nevertheless, multiple numerical simulations show that if the mass concentration is very high (a pronounced peak in the rotation curve) two waves with two different pattern speeds can coexist during some time in the galaxy. In this case the behavior is transient and it appears more appropriate to describe the kinematics of early-type galaxies. This scenario, which opens the possibility of the existence of two different pattern speeds in the central zone of a galaxy, where bars within bars can coexist, was shown through numerical simulations by Friedli & Martinet (1993). These scenarios with nested bars have been proposed as a gas fueling mechanism in active galactic nuclei and starbursts (Shlosman, Frank, & Begelman 1989; Shlosman, Begelman, & Frank 1990).

Theoretically, if a nuclear bar is formed via self-gravitational instability (in the stellar or gaseous disks), it must spin in the direction given by the angular momentum in the disk, i.e., in the direction of the primary bar (Shlosman et al. 1989). In this case, the pattern speed of the nuclear bar will be substantially higher than that of the primary bar. The best arrangement corresponds to the corotation radius of the nuclear bar being approximately equal to the radius of the inner Lindblad resonance (ILR) of the primary bar, reducing the fraction of chaotic orbits (Pfenniger & Norman 1990). The presence of gas appears to be imperative for this to occur (Shlosman 1999). In this case, both bars are dynamically decoupled and the angle between them in a face-on disk is arbitrary.

The problem of how bars are formed and evolve and their true role in the global evolutionary process of the system is directly related to the pattern speed of bar and to the position of the principal resonances in the disc. If the evolution of the bar is essentially a function of the accreted mass, then the pattern speed will vary with time and the Hubble sequence, under these circumstances, can also be a dynamic sequence, in which the galaxies evolve from late to early types. In this case the bars in the different types of galaxies should have different dynamic properties.

There are studies with N-body numerical simulations which indicate that the pattern speed of the bars depends on the ratio of masses of the bulge and the disc and on the scale length of the disc (Combes & Elmegreen, 1993). Therefore, the bars in late type galaxies should be limited by the scale length of the disc rather than by the resonances, contrary to early-type galaxies in which the bar would be limited essentially by corotation.

Self-consistent numerical simulations in 3D have been made of the evolution of isolated barred galaxies that consider stars, gas, stellar formation and radiative cooling separately (Friedli & Benz, 1993; 1995). These have shown that the bars can modify or influence the galaxy's dynamical evolution. The gravitational coupling between stellar bars and interstellar medium can fuel gas to the nucleus producing the destruction of the bar (appearance of a strong and extended inner Lindblad resonance). It appears, at this stage, that the presence of the bar does not affect the global star formation rate, but clearly does affect the circumnuclear region. Therefore, it appears that barred galaxies show a higher rate of stellar formation around the nucleus and generate the formation of more massive stars in the internal regions (Kennicutt 1994; Martin 1995; Ho, Filippenko, & Sargent 1995).

Recent barred galaxy surveys indicate that young bars in late-type spirals have a high stellar formation rate along the the mayor axis (Martin 1995). Nevertheless, within early type galaxies, it appears that the number of HII regions is much lower and they are found to be more loosely distributed around the nucleus.

NGC 3359 is a good candidate to perform comparisons between the observations and the theoretical predictions for barred galaxies: it is a barred spiral of grand design, isolated, with a very strong bar and a complex Hα structure, with many spectacular star formation regions concentrated in the bar and also distributed along the disc.

In this paper we have found a connection between the global dynamics and the morphology of star formation through the determination of the position of the main resonances in the disc. In § 2 we present a description of NHC 3359, in § 3 we present the numerical model and finally in § 4 we discuss the results found from a comparison of the galaxy observations in Hα and HI and numerical simulations.

2. NGC 3359; GLOBAL PROPERTIES

NGC 3359 is a grand-design spiral galaxy with a strong bar (see Figure 1), classified as SBc(s) 1.8 by Sandage & Tammann (1981) or as SBc(rs) by de Vaucouleurs et al. (1991). From its radial velocity of 1008 km s^{-1}, using H$_0$ = 75 km s^{-1} Mpc^{-1}, we derive a distance of 13.4 Mpc. Its complex morphol-

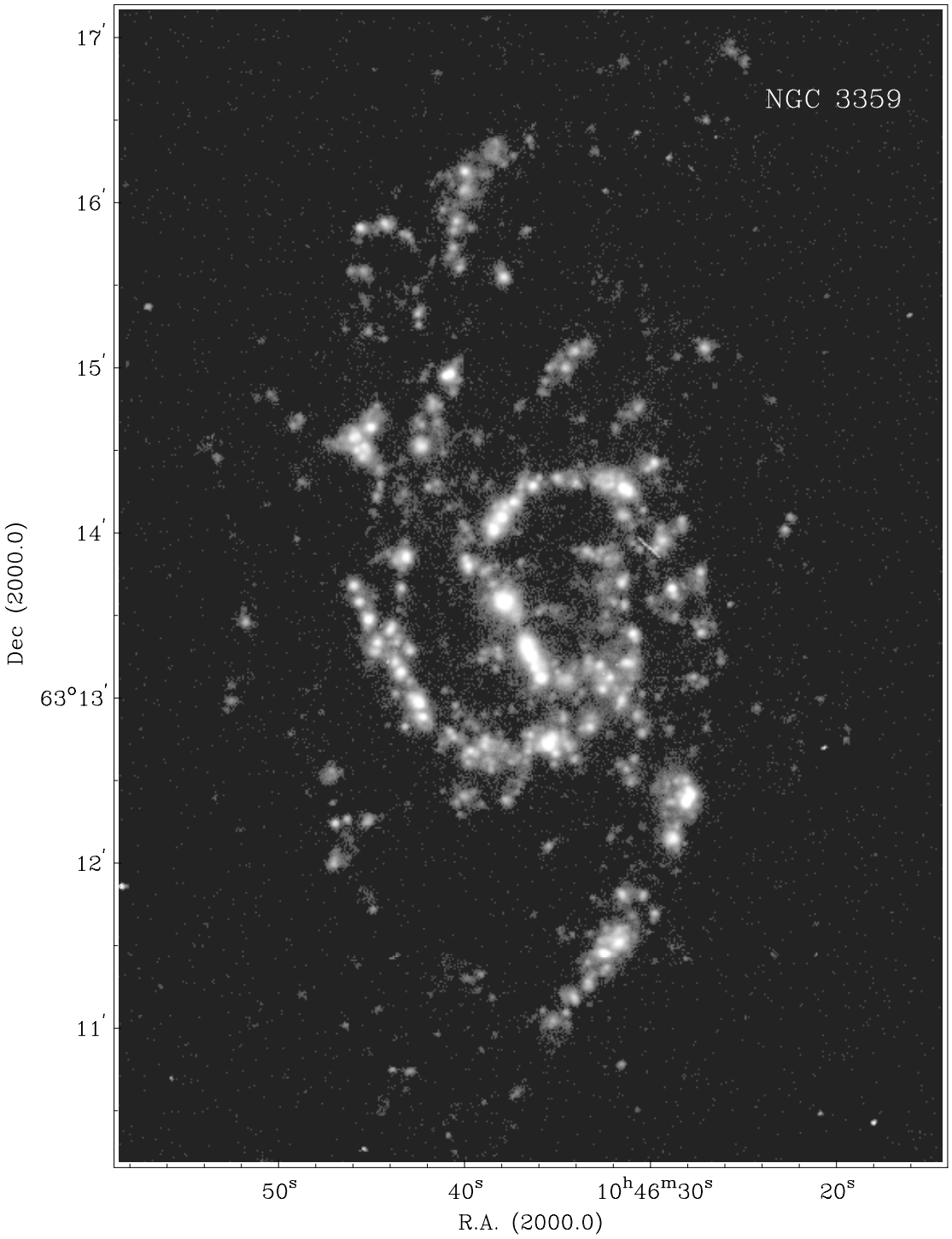

Fig. 1. Grey scale representation of the continuum-subtracted Hα image for NGC 3359.

ogy stands out if we analyze images taken at different wavelengths, showing prominent features. A strong main bar and an apparently misaligned nuclear bar (Figures 2b and 3b) are clearly seen in the I-band image. The Hα distribution in the inner 20″ region presents two prominent maxima misaligned with the main bar, underlining the absence of star formation in the nucleus.

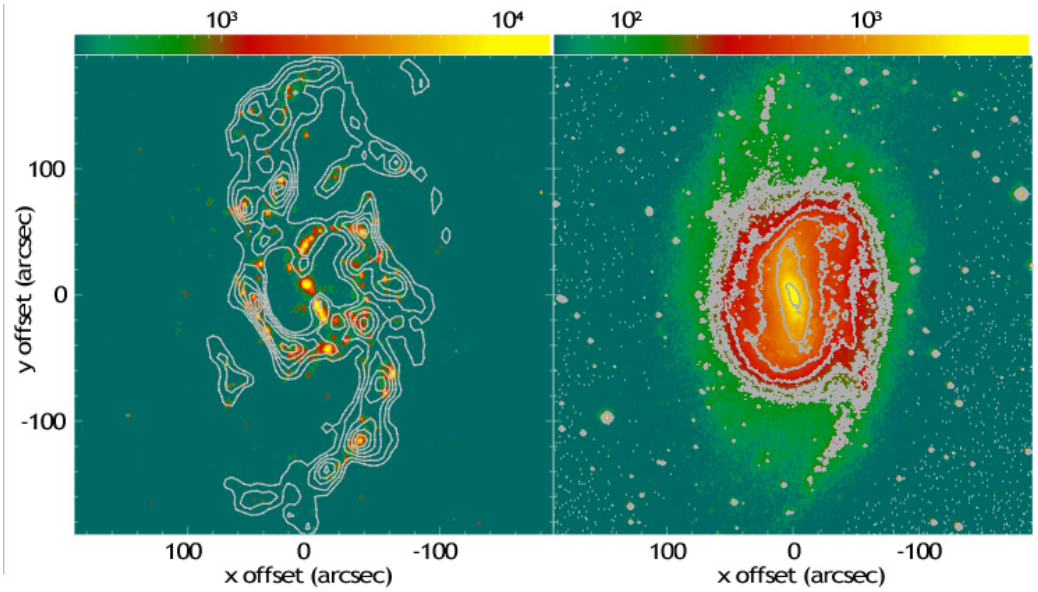

Fig. 2. (a) Overlay of Hα and HI images used for fitting the model. (b) I-band image from which we have derived the potential.

NGC 3359 was first observed in Hα by Hodge (1969), in the near IR by Elmegreen (1981), and in CO by Stark, Elmegreen, & Chaude (1987) and Braine & Combes (1992). The most detailed studies of this galaxy have been undertaken using Hα by Rozas, Zurita, & Beckman (2000a) and Rozas et al. (2000b). They analyze the distribution of the HII regions, their luminosities and other physical properties as well as the global kinematics of the galaxy. In Figure 1 we show a grey scale representation of the Hα continuum-subtracted image of NGC 3359. As we can see, it has well defined arms, well endowed with HII regions. The bar dominates the total Hα emission of the galaxy, in which we can see a chain of bright HII regions along its length and strong bursts of star formation at its end. Outside of the bar, the majority of the HII regions are concentrated within an annular zone, and there are many fainter regions along the spiral arms. The intensities of the arms are very disparate, the western arm being much brighter, bigger and better defined that the eastern arm. The slope of tha Hα luminosity function of the HII regions is within the range of values found previously for galaxies of similar type: $dNL = AL^{\alpha}dL$ with $\alpha = -1.69 \pm 0.06$.

The U-I map defines the detailed locations of star formation. In this map (Rozas et al. 2000a) we can see elongated segments of star formation and the "hot spots" which compose them, divided by dust, because the I-K image shows most clearly a spiral delineated by the strong dust lanes running along the arms.

The structure and kinematics of the neutral atomic hydrogen were analyzed in detail by Gottesman (1982) and by Ball (1986), with resolutions of $42'' \times 31''$ and 24.5 km s^{-1}, and $18''$ and 25 km s^{-1} respectively. The most significant results of these works were the distribution of the HI in clumps, and the low surface density within the annular zone of strong star formation, which can be explained by the effect of the bar, which sweeps up gas as it rotates. Ball (1992) produced a hydrodynamical analysis of the galaxy, reproducing the gas kinematics with models based on the stellar density in the bar, and he concluded that the spiral structure could not be reproduced from the non-axisymmetric potential obtained from the surface photometry of the stellar bar, since the force thus obtained falls off too quickly at large radii. In this model, he used a one pattern speed model and he had to add an oval component to obtain the extended outer spiral structure of the galaxy.

The bar of NGC 3359 has a deprojected total length of 2.9 arcmin (which corresponds to ~ 9 kpc). Around 17% of the total Hα flux from the galaxy comes from the bar. According to Friedli & Benz (1993) and to Friedli, Benz, & Kennicutt (1994) strong flows of gas are predictable along a bar which is at a formative stage. The hot spots in this case can be explained as due to star formation in the gas

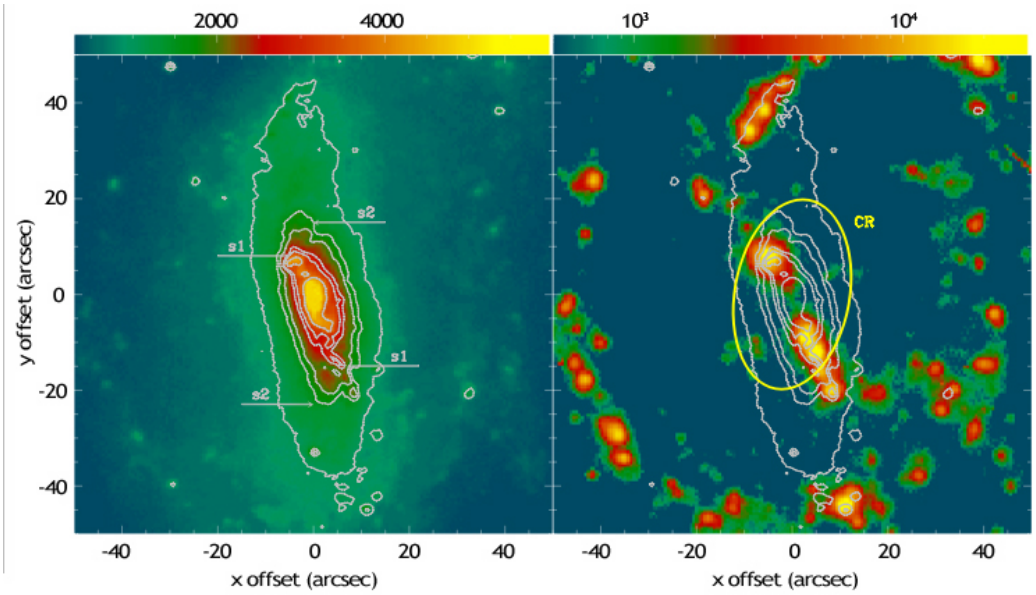

Fig. 3. (a) Zoom of the I-band image to show the two decoupled bars: two mini spiral leading arms (s1) start at the edges of the nuclear bar. (b) Contours of the I-bar superposed on the central Hα region. Note the two Hα maxima at the edges of the nuclear bar. The ILR of the slow mode (CR of the fast pattern) adopted in the numerical simulations is displayed as an ellipse.

which has not contributed to the intense star formation at the ends of the bar, due to interstellar shocks, but falls towards the centre as its angular momentum is absorbed in the shocks and in the more general bar potential. This gas can be trapped in the inner resonant structure of the galaxy, producing massive stars and hence the hot spots.

Properties of bars related to their velocity structures include their metallicity gradients. In a general study of metallicity gradients in galaxies, Vila Costas & Edmunds (1992) showed that the gradients within the bars of barred galaxies are much lower than those in the external discs. In NGC 3359, however, Martin & Roy (1995) found a higher gradient within the bar. They attributed this effect to the fact that in NGC 3359 the bar is still forming, so that there has not been time for turbulence to smooth out the intrinsic gradient due to a radially differential star formation rate. A related effect of this type of mixing in the disc is the reduced star formation symmetry in the arms of barred spirals compared with non-barred spirals, as reported in Rozas, Beckman, & Knapen (1998). The analysis of the non circular motions around the bar in Rozas et al. (2000b) explains the velocity gradients in this region as gas flowing in elliptical orbits around the bar. This, together with the presence in the bar region of strong star formation fits the general scenario of a bar in the process of formation.

TABLE 1

NGC 3359: BASIC PARAMETERS

R.A. (2000)	$10^h\ 46^m\ 37^s.7$
Dec (2000)	$63°\ 13'\ 22''$
Type	.SBT5..
D(Mpc)	13.4
log d_{25}	1.86
B_T	11.03
v_{opt}	1008 km s^{-1}
log r_{25}	0.22
P.A.	170

The first determination of a rotation curve was carried out by Ball (1986). This curve agrees well with the rotation curve in Hα derived by Rozas et al. (2000b), from high resolution data. In this paper we will use the Hα and I-band image taken by Rozas et al. (2000a) with the 4.2 m William Herschel telescope at the Roque de los Muchachos Observatory (Spain) to compare with the results of our numerical simulations. A detailed description of the observations can be found in Rozas et al. (2000a,b).

The global properties of the galaxy are set out in Table 1.

3. NUMERICAL MODELS

The numerical models applied to NGC 3359 have been used for the determination of the pattern speed in several grand-design galaxies: M 51 (García-Burillo, Combes, & Gerin 1993); NGC 4321 (García-Burillo, Sempere, & Combes 1994, and Sempere et al. 1994); NGC 7479 (Sempere, Combes, & Casoli 1995); NGC 157 (Sempere & Rozas 1997).

Numerical simulations of the molecular gas disc component have been carried out to fit observations in NGC 3359 and to derive the most important parameters of the density wave responsible of its bar and spiral structure. Our simulations are mainly non-self-gravitating, and molecular clouds are considered as test particles in the imposed potential. From a previous paper (Sempere et al. 1994) we have shown that the lack of self-gravity in the gas is not determinant for the large scale fit of the gas distribution, since this component accounts for less than 10% of the total mass in this galaxy, and its contribution to the total potential is negligible. Nevertheless, the shift of the gas shock relative to the center of the potential when self-gravity is included can be important when scale distances of the order of the spiral arm width are considered. Therefore, we have also included self-gravity in some runs.

We have performed two different runs of numerical simulations of the dynamical behavior of the molecular interstellar medium, namely:

- using the model of cloud inelastic collisions proposed by Combes & Gerin (1985), and
- using a modification of the previous model including de gas self-gravitation and partially inelastic collisions.

The models are designed to find the best global morphological fit between the molecular gas and the stellar disc potential, since the observations indicate that the distribution of molecular gas in isolated spiral galaxies follows the perturbation of the potential due to the bar and the spiral component. Nevertheless, the existence of ILRs in the inner region of a spiral galaxy can produce a shift between a gas bar and a stellar bar (Sanders & Tubbs 1980; Combes & Gerin 1985; Shaw et al. 1993). A detailed analysis of the gas behavior in the center of the galaxy would require a more sophisticated numerical model based on a polar grid which provides a higher spatial resolution at these radii.

The two main input parameters of the numerical simulations are the pattern speed of the bar + spiral perturbation, Ω_p, and the adopted mass distribution (or rotation curve). The accuracy of the method is based on the sensitivity of the model to the value of the pattern speed: very small variations of this parameter can change appreciably the final global morphologies.

In order to compare the model with the observations, we have performed the following steps:

- We need to derive the stellar potential for both runs of numerical simulations. The best tracer for this purpose would be an infrared image, but the I-band image is a good tracer of the mass distribution in normal spiral galaxies where dust absorption does not dramatically affect the red wavelengths. The I-band image, with a spatial resolution of $0\farcs59$/pixel and a seeing of $1''$, was cleaned of galactic stars and then projected in the plane of the galaxy assuming an inclination angle of 53°. The gravitational potential is computed using a Fast Fourier Transform method. We proceeded in two steps: first, assuming a constant M/L we converted the brightness distribution into a mass distribution and derived the rotation curve and the potential via the Poisson's equation. The FFT method uses a two dimensional Cartesian grid of 512 × 512 pixels of angular size $1'' \times 1''$, and we derived a rotation curve from the model, which is compared with the best curve obtained from interstellar Hα emission observations (Rozas et al. 2000b). In the second step, we fitted the profile necessary to obtain a surface density that corresponds to the observed rotation curve. To eliminate the uncertainty due to a bad determination of the rotation curve we will test the influence of different rotation curves in the final morphology obtained in the simulations. Finally, we adopted the curve obtained assuming a constant M/L ratio, as it seems more reliable than the central Hα and HI data. This point has been corroborated by a first run of simulations after adopting the observational curve from the gaseous tracers. Figure 4 shows the adopted rotation curve compared with that constructed from Hα and HI data.

  As simulations are performed in 3 dimensions, we extend the gravitational potential in a third direction z, perpendicular to the plane of the galaxy. For the sake of simplicity we assume cylindrical symmetry; thus, the gravitational forces in the plane (F_x and F_y forces) are independent of z. This assumption is based on the fact that the molecular gas disc is much thinner than the stellar disc. For the vertical forces, we

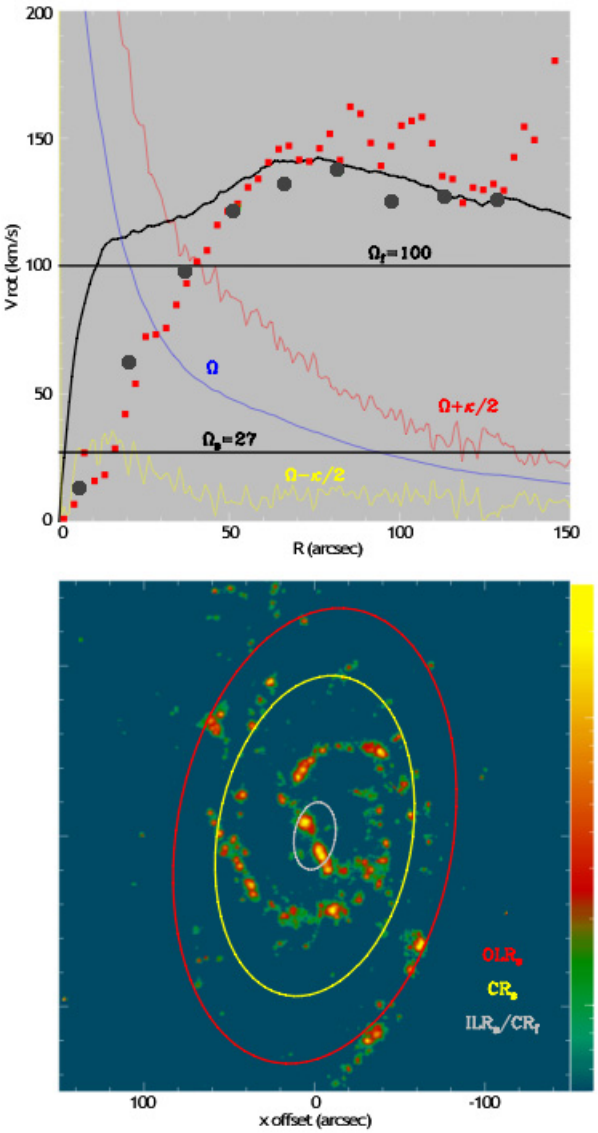

Fig. 4. (a) Adopted rotation curve. Filled and open squares are the Hα and HI observational data, respectively. The two pattern speeds are shown as straight lines. (b) The main resonances superposed on the Hα image.

assume that each stellar layer obeys the equilibrium of an infinite layer with a density law $\rho = \rho_0 sech^2(z/H)$, where we have adopted $H =$ 2 kpc as a characteristic height. The F_z forces are derived from this distribution. The forces calculated with this method do not satisfy Poisson's equation, but the length of the clouds is small and they do not make large excursions from the disk; thus, deviations from the real values can be neglected.

The gravitational potential, intended to closely approximate the real potential field, includes the spiral arms and the stellar bar. The next step consists of decomposing the total gravitational potential into its axisymmetric and non-axisymmetric parts. The symmetric part is the azimuthal average of the total potential for each radius. The non-axisymmetric component is obtained by subtraction of the axisymmetric part from the total potential, and represents the contribution of the spiral arms and stellar bar to the potential.

In both runs of numerical simulations we begin by launching molecular clouds in the axisymmetric potential with its rotational velocity and giving the clouds a small velocity dispersion of 10 km s^{-1}. The non-axisymmetric potential is introduced gradually with a 20% delay of the total time of the run (7.8×10^8 years) and with a constant pattern speed Ω_p.

- In the first model a total number of 4×10^4 clouds are distributed according to a mass spectrum ranging from 10^3 to 10^6 $M_\odot$ (Casoli & Combes 1982), and their scale follows a $(M_{cloud})^{1/2}$ law, as is typical for an ensemble of molecular clouds (e.g. Solomon et al. 1987). The initial radial distribution is an exponential disc of scale length $a_d = 3.8$ kpc and the distribution perpendicular to the plane is Gaussian, as expected from the equilibrium of a multi-component system.

  The clouds, modelled as spheres, move as test particles in the stellar potential computed from the I-band image, and interact via inelastic collisions, whose final results can be coalescence, mass exchange or fragmentation, the total mass being conserved during the run. The energy lost by collisions is re-injected via simulated star formation events: after a GMC life-time of 4×10^7 years, very large clouds (with masses bigger than $3 \times 10^5 M_\odot$) are disintegrated into a collection of small clouds which are reinjected in the interstellar medium with a random velocity of 10 km s^{-1}. This velocity dispersion balances the energy lost in the collisions and ensures the stability of the cloud distribution in an axisymmetric disc. The total simulation time of a run is 7.4×10^8 years. After this time molecular gas has been trapped into the potential well created by the non-axisymmetric structure and has reached a quasi-stationary state.

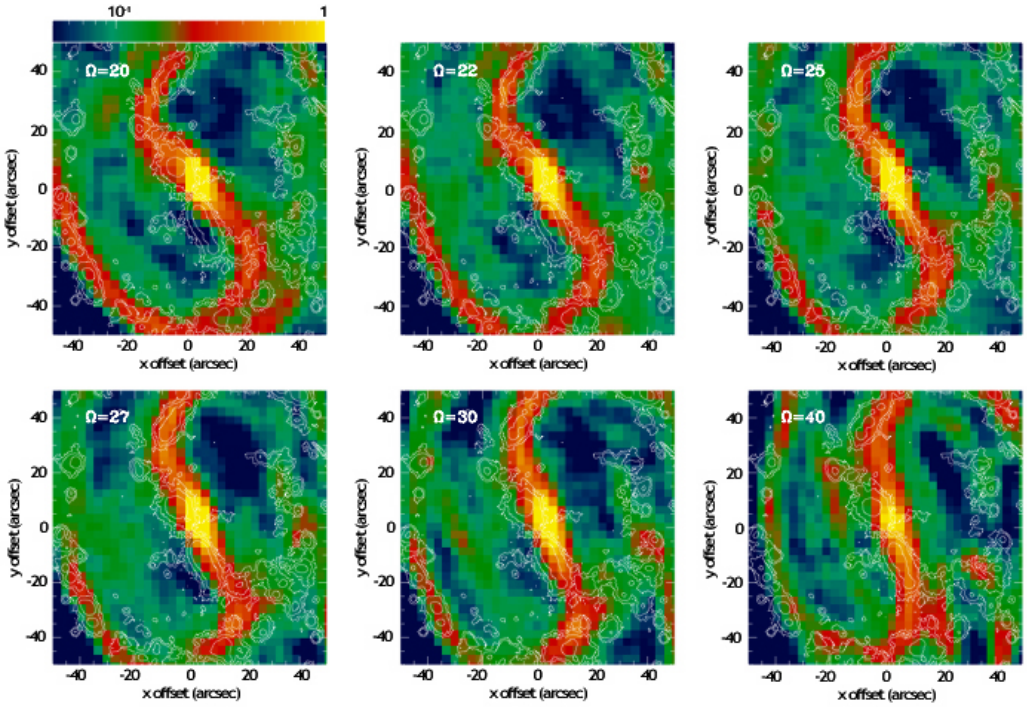

Fig. 5. Contours of the Hα image superposed on the results of the numerical simulations performed with a unique pattern speed for different values of the angular velocity. The central bar is not fitted by the model and, particularly, the nuclear structure is not reproduced.

- In the second model we introduced the self gravity of the gas in order to better analyze the behavior of the gas in the center of the galaxy. The total stellar mass inferred from our red image is $M_\star = 3.9 \times 10^{10} M_\odot$. The influence due to gas self-gravitation in the global disc could not be very important if $M_g/M_\star \leq 0.1$ (Wada & Habe 1992; Friedli & Benz 1993). Braine & Combes (1992) calculate a $\log M_{H_2} = 7.4$ for the nucleus (inner kpc). They note the fact that this galaxy does not present strong CO emission in the center. The neutral hydrogen mass of NGC 3359 detected by Gottesman (1982) is $0.015 \times 10^9 \times D^2$, or $2.7 \times 10^9 M_\odot$ for $D = 13.4$ Mpc; and if we assume a normal ratio of molecular to atomic gas for late type spirals, we can suppose that the influence due to gas self-gravitation is not important. To obtain a clear picture of the simulation plots we have suppressed the star formation events to better follow the particle orbits. We have arbitrarily assumed all clouds to have the same mass: $10^3 M_\odot$. Clouds interact via partially inelastic collisions. The value of the inelasticity parameter in the direction parallel to the relative velocity between two colliding clouds is ~ 0.65 and 1 in the direction perpendicular to the encounter to assure the conservation of the angular moment. The gravitational forces due to the gas have been computed by an FFT method and added to the imposed stellar potential (Combes et al. 1990).

4. COMPARISON BETWEEN THE MODEL AND THE OBSERVATIONS

After each run we store the positions projected on the plane of the sky, and the radial velocities of the clouds. Then, to compare the results of our models with the images, we produce simulated maps of the molecular gas under the assumption that the interstellar medium is optically thin in clouds (i.e. the molecular cloud crowding factor is low for all cloud velocities).

A data cube is built by convolving the expected emission of the clouds using a telescope beam halfwidth of 12″.The cell size of the cube is $6'' \times 6''$ in the spatial dimensions and 3 km s^{-1} in velocity. We have carried out several runs with different Ω_p values. At first, we tried a unique pattern speed, though the inner morphology is not matched by the model. In Figure 5 we show contours of the Hα image superposed on the results of the numerical simulations performed with a unique pattern speed for

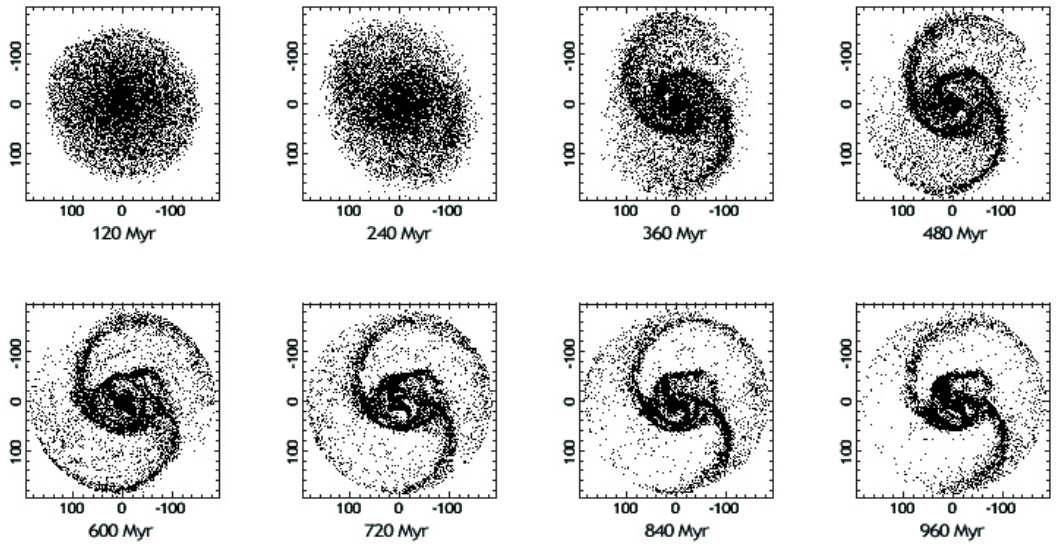

Fig. 6. Different steps of the numerical simulations from 120 to 960 Myr of the two pattern speed model, with the adopted Ω_s = 27 km s^{-1} kpc^{-1} for the slow main bar + outer spiral and Ω_f = 100 km s^{-1} kpc^{-1} for the nuclear bar.

different values of Ω_p. The central bar is not fitted by the model and, particularly, the nuclear structure is certainly not reproduced.

A spiral structure similar to that observed is obtained only for a model with two different pattern speeds. The best fit is obtained when the non-axysimmetric potential component is divided in two parts representing two decoupled bars with different angular velocities: the main + outer spiral, which is introduced in the simulations with a delay of 150 Myr, and the nuclear bar. The two pattern speeds that best reproduce the observations are Ω_s = 27 km s^{-1} kpc^{-1} and Ω_f = 100 km s^{-1} kpc^{-1} respectively. The choice of the angular speeds is constrained by the location of the resonances: the corotation of the fast pattern is in the ILRs region of the slow one (Tagger et al. 1987). Figure 4 shows the two circular angular velocities and the Lindblad precession frequencies, $\Omega - \kappa/2$ and $\Omega + \kappa/2$, versus radius. In this figure we show the radii of the main resonances overlaid on the Hα image: the corotation radius for the Ω_s = 27 km s^{-1} kpc^{-1}, where the angular velocity of the matter Ω is equal to the pattern speed of the density wave, is located at a radius of 95″ in the middle of the optical disc. An outer Lindblad resonance is located in the outer disc at a radius of 130″, and an IRLs zone is situated at a radius of 20″: the same place of the corotation radius of the fast pattern speed as the theory predicts.

Figure 6 shows different steps of the numerical simulations from 120 to 960 Myr with the adopted Ω_s = 27 km s^{-1} kpc^{-1} for the slow main bar + outer spiral and Ω_f = 100 km s^{-1} kpc^{-1} for the nuclear bar. The overlays of the HI contours map and the Hα image on the modelled intensity map obtained from the self gravitating model are displayed in Figures 7a and 7b, respectively, to show the agreement with the outer spiral. In both cases the best fit is obtained for the two pattern speeds mentioned above.

A quantitative comparison of the results of the simulations and the Hα image by a linear regression method gives the correlation coefficients shown in Table 2. The method used consists in creating a convolution integral F(n,o)=$I_{model(x,y)}$*$I_{obs(x,y)}$*W(x,y), where I_{model} and I_{obs} are the intensities of the model and the real image, respectively, and W(x,y) is a weight function which measures how well the model matches the real image. W(x,y) is largest where the data are best measured. When we calculate the mean intensity and subtract it from the function and normalize the convolution so that F(n, n) = F(o,o) = 1, then F changes between −1 and +1, −1 representing the worst value and +1 the best value of the match. We can see from the numbers in Table 2, that the models with Ω_s=27 and Ω_f=100 and 105 have the same correlation, and that the model with Ω_s=29 is almost as good. Looking at those numbers, we would say that both Ω_f and Ω_s are uncertain to at least ±5%, and more likely ±10%. But examining the models by eye, we conclude that the best results are the above mentioned values. The row of negative

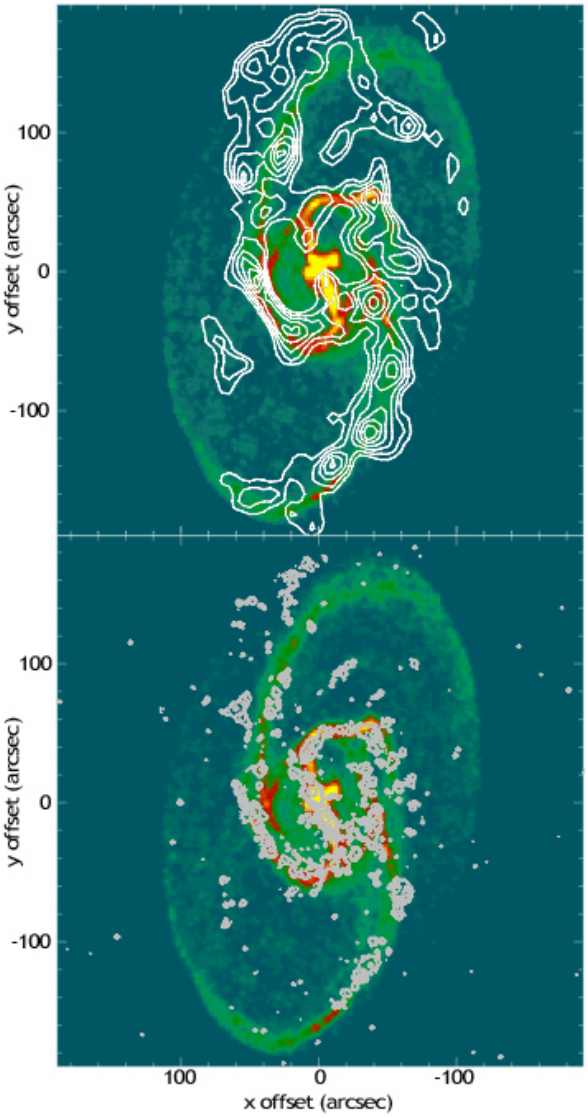

Fig. 7. (a) Overlay of the HI contour map on the best fit of the numerical simulations. We can see the agreement with the outer spiral. (b) The same for the Hα image.

numbers in the column for 90 km s^{-1} kpc^{-1} is then quite striking but can be easily interpreted: periodic orbits change its orientation by 90° when they cross over a resonance.

Figure 8a shows the central part of the galaxy: Hα contours of the central bar superposed on the best fit of the numerical simulations; the two peak maxima and the mini spiral are both present in the model. Figure 8b is a overlay of the velocity field (contours) with the modeled gas distribution. We can see strong streaming motions delineating a patchy spiral structure; which agree with the velocity gradients around the bar found by Rozas et al. (2000b) in the Hα kinematics, and explained as highly oval gas circulation driven by the barlike potential field in the inner parts. This, together with the presence in the bar region of strong star formation fits the general scenario of a bar in the process of formation. This scenario agrees with the classification of NGC 3359 as a late-type spiral, but the fact that the global dynamics corresponds to a two pattern speed model in the central zone of the galaxy, where two nested bars can coexist shows this galaxy to be more related to early-type galaxies.

TABLE 2

CORRELATION COEFFICIENTS OF THE LINEAR REGRESSION

Ω_s \ Ω_f	85	90	95	100	105	110	115
21	0.52	−0.54	0.58	0.70	0.69	0.56	0.54
23	0.61	−0.64	0.68	0.72	0.71	0.67	0.64
25	0.56	−0.65	0.68	0.72	0.70	0.66	0.63
27	0.58	−0.64	0.74	0.77	0.77	0.67	0.64
29	0.60	−0.60	0.69	0.76	0.74	0.64	0.59
31	0.59	−0.56	0.68	0.73	0.71	0.62	0.57

Figure 9 shows the particle orbits in the nuclear region from a frame rotating at $\Omega_s = 27$ km s^{-1} kpc^{-1} for the best fit resolution of the two pattern model.

Heller, Shloaman, & Englmaier (2001) performed an analysis of the characteristics of non-self-gravitating gaseous bars in barred galaxies, and their formation from nuclear rings and decoupling from the underlying gravitational potential. They found that the degree of viscosity in the gas to be a crucial factor in the diverging evolution of these systems. The low-viscosity systems are expected to spend a substantial period of time in a fully decoupled state, with nuclear gaseous bars having much slower pattern speeds compared to the primary bars. They also find it plausible that gas compression accompanying such decoupling, can be associated with bursts of star formation and with gas circulation across the ILRs, as is observed in NGC 3359 from its kinematics (Rozas et al. 2000b). NGC 3359 appears to be a galaxy with both these dynamical and morphological characteristics.

From the determination of the position of the main resonances in other late-type spirals such as NGC 4321, NGC 7479 and NGC 157, we have found very different kinematical characteristics that determine a large variety of bar properties and star formation processes. Although NGC 4321 has been classified as late-type, its kinematical behavior cor-

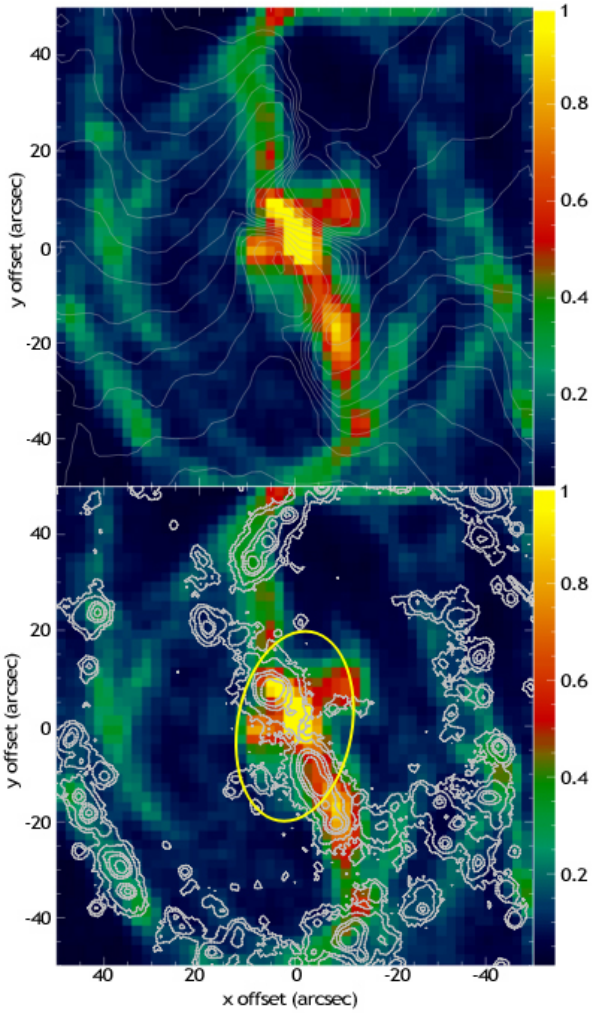

Fig. 8. (a) Hα central zone of the galaxy (contours) superposed on the best fit of the model: The two peaks (maxima) and the mini spiral are both present in the model. (b) Overlay of the velocity field (contours) on the modeled gas distribution.

responds more to that of an early-type galaxy. On the contrary, NGC 7479 shows the bar characteristics and pattern speed predicted for a late-type by Combes & Elmegreen (1993). NGC 157 could be an intermediate case, since its dynamics follow the general trend of late types, but it has some characteristics of early-type galaxies, such as a local maximum at the center of the its rotational curve.

Thus, we can find very different dynamical behavior in spirals of the same type. It seems more appropiate to classify spiral galaxies on the basis of both their kinematical and morphological properties.

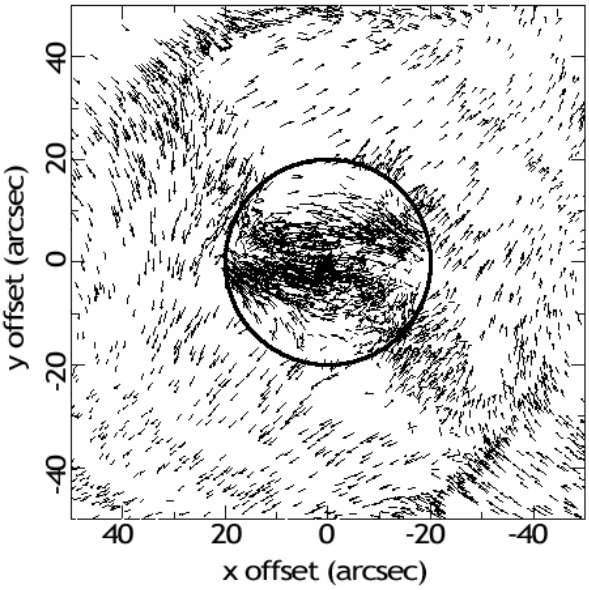

Fig. 9. A frame for the best fit solution of the two pattern speed model showing the particle orbits in the central region.

5. CONCLUSIONS

We have carried out numerical simulations in order to determine the pattern speed of the density wave responsible for the bar plus spiral structure of NGC 3359. The idea is that the family of periodic orbits is completely different in a given stellar potential, with different pattern speeds: the gas tends to follow different orbits, and the resulting morphology can depart significantly from the observed morphology, if the chosen pattern speed is far from the real one.

The most sensitive parameters in the numerical simulations are the pattern speed of the wave, and the mass distribution in the galaxy, which produces the rotation curve. Since we have obtained the mass distribution from a red image of the galaxy with some assumptions about mass to light ratio, the only free parameter that we vary in our simulations is Ω_p. We have run two models: the first one is a model of inelastic cloud collisions without self-gravity, in which the effects of star formation are simulated. The second model considers partially inelastic collisions, suppresses the star formation events and includes the gas self-gravity in order to analyze in more detail the gas behavior at the center and in the arms of the galaxy, where gas self-gravity can play an important role.

The results of numerical simulations have been compared with a set of observations (Hα, HI) to

search for the best fit. We summarize the main results of this work as follows:

1. We have tried to fit the morphology of the galaxy to a model constructed with a unique pattern speed, with different values of Ω_p. The nuclear structure of the galaxy cannot be reproduced by the model.

2. The best morphological fit is found for a two pattern speed model representing two decoupled bars with different angular velocities: the main bar + outer spiral rotates with a $\Omega_s = 27$ km s^{-1} kpc^{-1}, and the nuclear bar with a $\Omega_f = 100$ km s^{-1} kpc^{-1}.

3. The corotation radius for the slow pattern speed is located at a radius of 95″ in the middle of the optical disc. An outer Lindblad resonance is located in the outer disc at a radius of 130″, and an IRLs zone is situated at a radius of 20″: the same place of the corotation radius of the fast pattern speed, as the theory predicts.

4. Our simulations reproduce the Hα and HI observations, including the inner structures: the twin peak maxima and the mini-spiral are present in the model.

5. The analysis of the non circular motions around the bar in Rozas et al. (2000b) explains the velocity gradients in this region as gas flowing in elliptical orbits around the bar. This, together with the presence in the bar region of strong star formation, fits the general scenario of a bar in the process of formation.

6. The dynamical model proposed for NGC 3359 is confirmed by the morphology. From this model we suggest that NGC 3359 is a low-viscosity system (Heller et al. 2001) which spends a substantial time in a decoupled state, with a nuclear bar having a much slower pattern speed that the main bar. In this case we expect bursts of star formation and gas inflow across the IRLs, related with gas compression accompanying this decoupling.

7. NGC 3359, classified as a late-spiral galaxy, does not show the typical bar characteristics and pattern speed predicted for a typical bulge-less galaxy (Combes & Elmegreen 1993). The global dynamics in the central zone of the galaxy, where two nested bars can coexist, relates this galaxy rather to the early-type galaxies. Nevertheless, the presence of a bar in a formation stage with strong star formation, is rather more associated with the late-type spirals. From the determination of the position of the main resonances in this galaxy and in other late-type spirals we found a very different dynamical behavior in spirals of the same type: it would be more adequate to classify spiral galaxies on the basis of both their kinematical and morphological properties.

REFERENCES

Ball, R. 1986, ApJ, 307, 453
_____. 1992, ApJ, 395, 418
Braine, J., & Combes, F. 1992, A&A, 264, 433
Casoli, F., & Combes, F. 1982, A&A, 198, 43
Combes, F., Debbasch, F., Friedli, D., & Pfenniger, D. 1990, A&A, 233, 82
Combes, F., & Elmegreen, B. G. 1993, A&A, 271, 391
Combes, F., & Gerin, M. 1985, A&A, 150, 327
de Vaucouleurs, G., de Vaucouleurs, A., Corwin, H. G., Buta, R. J., Paturel, G., & Fouque, P. 1991, Third Reference Catalogue of Bright Galaxies (RC3) (New York: Springer)
Elmegreen, D. M. 1981, ApJS, 47, 229
Erwin, P., & Sparke, L. 1999, ApJ, 521, L37
Friedli, D., & Benz, W. 1993, A&A, 268, 65
_____. 1995, A&A, 301, 649
Friedli, D., Benz, W., & Kennicutt, R. 1994, ApJ, 430, L105
Friedli, D., & Martinet, L. 1993, A&A, 277, 27
Friedli, D., Wozniak, H., Rieke, M., Martinet, L., & Bratschi, P. 1996, A&AS, 118, 461
García-Burillo, S., Combes, F., & Gerin, M. 1993, A&A, 274, 148
García-Burillo, S., Sempere, M. J., & Combes, F. 1994, A&A, 287, 419
Gottesman, S. T. 1982, AJ, 87, 751
Heller, C., Shloaman, I., & Englmaier, P. 2001, ApJ, 553, 661
Ho, L. C., Filippenko, A. V., & Sargent, W. L. W. 1995, ApJS, 98, 477
Hodge, P. W. 1969, ApJS, 18, 73
Kenney, J. D. 1998, in IAU Symp. 184, The Central Regions of the Galaxy and Galaxies, ed. Y. Sofue (Boston: Kluwer), 43
Kennicutt, R. C. 1994, in Mass-Transfer Induced Activity in Galaxies, ed. I. Shlosman (New York: Cambridge Univ. Press), 131
Maciejewski, W., & Sparke, L. S. 2000, MNRAS, 313, 745
Maiolino, R., Alonso-Herrero, A., Anders, S., Quillen, A., Rieke, M. J., Rieke, G. H., & Tacconi-Garman, L. E. 2000, ApJ, 531, 219
Martin, P. 1995, AJ, 109, 2428
Martin, P., & Roy, J. R. 1995, ApJ, 445, 161
Pfenniger, D., & Norman, C. A. 1990, ApJ, 363, 391

Rozas, M., Beckman, J. E., & Knapen, J. H. 1998, MNRAS, 301, 631
Rozas, M., Zurita, A., & Beckman, J. E. 2000a, A&A, 354, 823
Rozas, M., Zurita, A., Beckman, J. E., & Pérez, D. 2000b, A&AS, 142, 259
Sandage, A., & Tammann, G. A. 1981, A Revised Shapley-Ames Catalog of Bright Galaxies (Washington: Carnegie Inst.)
Sanders, R. H., & Huntley, J. M. 1976, ApJ, 209, 53
Sanders, R. H., & Tubbs, A. D. 1980, ApJ, 235, 803
Sempere, M. J., Combes, F., & Casoli, F. 1995, A&A, 299, 371
Sempere, M. J., García-Burillo, S., Combes, F., & Knapen, J. H. 1994, A&A, 296, 45
Sempere, M. J., & Rozas, M. 1997, A&A, 317, 405
Shaw, M. A., Axon, D. J., Probst, R., & Gatley, I. 1995, MNRAS, 274, 369
Shaw, M. A., Combes, F., Axon, D. J., & Wright, G. S. 1993, A&A, 273, 31
Shlosman, I. 1999, in ASP Conf. Ser. 187, Evolution of Galaxies on Cosmological Timescales, ed. J. E. Beckman & T. J. Mahoney (San Francisco: ASP), 100
Shlosman, I., Begelman, M. C., & Frank, J. 1990, Nature, 345, 679
Shlosman, I., Frank, J., & Begelman, M. C. 1989, Nature, 338, 45
Solomon, P. M., Rivolo, A. R., Barret, J. W., & Yahil, A. 1987, ApJ, 319, 730
Stark, A. A., Elmegreen, B. G., & Chaude, D. 1987, ApJ, 322, 679
Tagger, M., Sygnet, J. F., Athanassoula, E., & Pellat, R. 1987, ApJ, 318, L43
Vila Costas, M. B., & Edmunds, M. G. 1992, MNRAS, 259, 121
Wada, K., & Habe, A. 1992, MNRAS, 258, 82

M. Rozas: Instituto de Astronomía, Universidad Nacional Autónoma de México, Apdo. Postal 877, 22830 Ensenada, B. C., Mexico (maite@astrosen.unam.mx).